Hierarchical Polymer–Drug Nanoplatform with Polydopamine Shell and Folate Targeting for Synergistic Cancer Therapy

Loredana E. Nita[1], Alexandru-M. Serban[1], Alina Ghilan[1], Alina Gabriela Rusu[1], Isabella Nacu[2], Liliana Verestiuc[2], Aurica P. Chiriac[1]

[1] Department of Natural Polymers, Bioactive and Biocompatible Materials, "Petru Poni" Institute of Macromolecular Chemistry, 41-A Grigore Ghica Voda Alley, 700487 Iasi, Romania

[2] Biomedical Sciences Department, Faculty of Medical Bioengineering, "Grigore T. Popa" University of Medicine and Pharmacy of Iasi, 9-13 Kogalniceanu Street, 700454 Iasi, Romania

Abstract

The clinical performance of paclitaxel (PTX) remains limited by poor tumor selectivity, systemic toxicity, and rapid clearance. In this study, we report the development of multifunctional polymeric nanoemulsions based on poly(ethylene brassylate-co-squaric acid) (PEBSA_Brij) designed for targeted and controlled anticancer delivery. The copolymer matrix integrates hydrophobic domains for PTX encapsulation and polar squaric acid moieties to enhance intermolecular interactions and structural tunability. Surface functionalization with polydopamine (PDA) enabled subsequent folic acid (FA) conjugation, aiming to promote receptor-mediated uptake in folate receptor–overexpressing breast cancer cells.

Nanoemulsions with controlled size (170–181 nm), low polydispersity, and good colloidal stability were successfully obtained. Spectroscopic analyses confirmed polymer-drug interactions and surface modification. Antioxidant evaluation demonstrated radical scavenging capacity associated with the PDA layer, while loading of PTX enabled therapeutic potential. Biological evaluation on MCF-7 cells revealed enhanced cytotoxicity for FA-functionalized PTX-loaded nanoemulsions compared to non-targeted formulations, suggesting improved cellular internalization. At 24 h, $PEBSA_1$/PDA/FA/PTX (25/75) demonstrated the most rapid onset of cytotoxicity, with cell viability decreasing to approximately 90% at 5 mg/mL. The developed platform combines structural versatility, targeting capability, and dual-drug loading potential, highlighting PEBSA-based nanoemulsions as promising candidates for advanced breast cancer nanotherapy.

Keywords: nanocarriers, nanoemulsions, paclitaxel, cancer therapy

1. Introduction

Cancer chemotherapy remains limited by insufficient tumor selectivity, rapid systemic clearance, premature drug degradation, and severe off-target toxicity, which collectively reduce therapeutic efficacy and patient compliance. Conventional administration of highly potent cytotoxic agents such as PTX often requires high systemic doses to achieve therapeutic concentrations at the tumor site, resulting in dose-limiting side effects including neurotoxicity, myelosuppression, and multidrug resistance development [1]. Consequently, the design of multifunctional nanocarrier systems capable of protecting labile drugs, enabling controlled release, and improving tumor-specific accumulation has become a central focus in modern oncological nanomedicine [2]. The limitations of conventional PTX chemotherapy, including systemic toxicity and rapid clearance, have been widely reported [3–6]. Polymeric nanocarriers represent an attractive platform for anticancer drug delivery due to their structural versatility, tunable degradation behavior, and high loading capacity for hydrophobic therapeutics. In this context, poly(ethylene brassylate)-based materials have recently attracted interest owing to their favorable biocompatibility, mechanical flexibility, and hydrophobic character, which support sustained drug encapsulation and prolonged release profiles [7]. However, purely hydrophobic polymer matrices often suffer from limited functional tunability and insufficient interaction with drug molecules, leading to suboptimal encapsulation efficiency and uncontrolled release kinetics [8,9]. The incorporation of squaric acid units into the polymer backbone introduces polar functional domains capable of hydrogen bonding and dipole-dipole interactions, thereby improving polymer-drug affinity and enabling modulation of release behavior. Moreover, the presence of squaric acid moieties may impart pH-responsive characteristics that are particularly relevant in the acidic tumor microenvironment, offering an additional level of therapeutic control.

Beyond carrier design, combination chemotherapy strategies have emerged as an effective approach to overcome tumor heterogeneity and drug resistance. PTX remains one of the most widely used microtubule-stabilizing agents in clinical oncology; however, its therapeutic potential is often compromised by intrinsic or acquired resistance mechanisms [10]. Retinoids such as retinyl acetate (RA) have demonstrated the ability to modulate gene expression through

retinoic acid receptor (RAR)-mediated pathways, promoting cellular differentiation, suppressing oncogenic signaling, and sensitizing cancer cells to chemotherapeutic agents. Previous studies have shown that retinoid-based co-therapy can enhance apoptosis induction and reduce chemoresistance when combined with microtubule-targeting drugs. Therefore, the co-delivery of PTX and RA within a single nanocarrier platform represents a rational strategy to achieve synergistic anticancer effects by simultaneously targeting cytoskeletal dynamics and transcriptional regulation pathways. Retinoid-mediated gene regulation combined with microtubule inhibition offers synergistic anticancer effects [11–14].

Despite these advances, the therapeutic performance of polymeric nanocarriers is still strongly affected by premature drug leakage, instability in biological fluids, and rapid opsonization by the immune system. To address these limitations, bioinspired surface engineering approaches have gained increasing attention. Polydopamine (PDA), inspired by mussel adhesive proteins, offers a versatile coating platform characterized by strong interfacial adhesion, excellent biocompatibility, and multifunctional chemical reactivity, photo-thermal conversion ability, and high loading of components [15]. PDA shells can effectively protect encapsulated drugs from degradation, suppress burst release phenomena, and improve nanoemulsions colloidal stability in physiological environments. Additionally, the intrinsic pH-responsive behavior of PDA enables accelerated drug release under acidic conditions, further enhancing tumor-selective delivery. Polydopamine coatings provide bioinspired protection and pH-triggered release capabilities [16–19]. Also PDA has been developed as a promising carrier for drug delivery in cancer therapy due to its intrinsic properties [20,21].

Targeted drug delivery represents another crucial element for maximizing therapeutic efficacy while minimizing systemic toxicity. Among various targeting ligands, FA has emerged as a particularly attractive candidate due to its small molecular size, low immunogenicity, and high affinity for folate receptor-α, which is overexpressed in a wide range of solid tumors. FA targeting becomes one of the most clinically validated active targeting strategies [22–24]. FA functionalization enables receptor-mediated endocytosis, facilitating enhanced intracellular accumulation of nanocarriers in cancer cells while sparing healthy tissues. When combined with a protective PDA shell, FA conjugation can be achieved in a straightforward and stable manner, preserving targeting efficiency without compromising nanoemulsion integrity [25–28]. Thus, the nanoemulsions are proper for cancer rehabilitation, and can reverse the immunosuppressive

environment at the tumor site with good beneficial effects on the beginning, development, and metastasis of tumors [29].

Recently, our group reported a new polymer structure, poly(ethylene brassylate-co-squaric acid) (PEBSA_Brij), synthesized by emulsion polymerization technique via ethylene brassylate ring opening (EB) followed by polycondensation with acid squaric (SA) units [30]. The copolymer was found to be biocompatible, with amphiphilic behavior and affinity for encapsulation of hydrophobic bioactive drugs. In addition, PEBSA_Brij has the capacity to self-assemble into globular structures, determined by a specific organization of the carbonyl functional groups of SA [31,32]. Oil-in-water (O/W) nanoemulsions of PEBSA_Brij, loaded with levofloxacin, have also been reported, which exhibit dual therapeutic effect and applicability as an ophthalmic drug delivery system [33].

In this work, we report the development of a hierarchical multifunctional nanoplatform based on PEBSA_Brij co-loaded with PTX and RA, subsequently coated with PDA and functionalized with FA. This integrated architecture combines structural polymer engineering, synergistic co-drug therapy, bioinspired surface protection, and receptor-mediated targeting within a single system. To the best of our knowledge, this is the first report exploiting PEBSA_Brij copolymers as multifunctional nanocarriers for PTX combined with PDA-based targeting interfaces.

The proposed nanoplatform is designed to simultaneously address multiple critical barriers in cancer drug delivery: (i) enhanced encapsulation efficiency and controlled release enabled by the tailored polymer matrix, (ii) improved therapeutic efficacy through synergistic drug co-delivery, (iii) increased colloidal stability and protection against premature drug degradation provided by the PDA shell, and (iv) selective tumor uptake mediated by FR targeting. This rational multi-component design offers a promising strategy for next-generation anticancer nanotherapeutics with improved efficacy and reduced systemic toxicity.

2. Materials and methods

2.1. Materials

Ethylene brassylate (EB, 1,4-dioxacycloheptadecane-5,17-dione, $C_{15}H_{26}O_4$, Mw = 270.36 g/mol, purity (GC) > 95.0%), squaric acid (SA, 3,4-dihydroxy-3-cyclobutene-1,2-dione, $H_2C_4O_4$,

Mw = 114.06 g/mol, purity (HPLC) > 99.0%), Dopamine hydrochloride (DOPA) (2-(3,4-Dihydroxyphenyl)ethylamine hydrochloride, $C_8H_{12}ClNO_2$, Mw = 189.64) and Tween 80 (polyoxyethylenesorbitan monooleate) were purchased from Sigma-Aldrich Co., (Darmstadt, Germany); Vitamin A in the form of retinyl acetate solution, 1 mL solution − 20.054 mg retinyl acetate ($C_{22}H_{32}O_2$) in sunflower oil, and sodium bicarbonate ($NaHCO_3$) were purchased from a local pharmacy, Iași, Romania; PTX ($C_{47}H_{51}NO_{14,}$ Mw = 853.92, purity HPCL>98.0%) from Tokyo Chemical Industry Co (Tokyo, Japan); anhydrous 1-hexanol from Acros-Organics (Geel, Belgium), Brij 58 (polyoxyethylene (20) cetylether, HO-(CH_2CH_2O)n-(CH_2)15-CH_3) from Merck (Hohenbrunn, Germany); Ethanol (C_2H_6O, Mw = 46,068 g/mol) from Chemical Company (Iasi, Romania). All the reagents were used without further purification. The ultrapure water used in all experiments was prepared with a Milli-Q device.

2.2 Copolymer synthesis

The synthesis of PEBSA_Brij copolymer has been previously presented in detail [30,33]. Briefly, the copolymers were obtained by aqueous emulsion polymerization technique using Brij 58 as the surfactant, through the ring opening of EB in the presence of 1-hexanol as initiator, followed by condensation with SA units. Three copolymer variants were chosen for this study (Table S1). At the end of the reaction, the copolymer was poured into ice-cold water and separated by centrifugation. Subsequently, the copolymer was washed several times with distilled water and then lyophilized for analysis and further use.

2.3. Nanoemulsion preparation

2.3.1 PEBSA/PDA nanoemulsions

PEBSA/PDA nanoemulsions were prepared using a single oil-in-water emulsion technique. An example is shown below: first, a mixture of 0.01 g PEBSA_Brij and retinol acetate (12000 IU/8 mg) dissolved in 0.4 ml sunflower oil was prepared. The resulting solution was then added dropwise to 10 ml of a 0.6% w/v Tween 80 solution in Tris-HCl buffer. After 1 h, 0.01 g of DOPA was added. The samples were left under vigorous stirring (1400 rpm) for 24 hours for oxidation-induced self-polymerization of dopamine (PDA) in an alkaline medium and were characterized using DLS technique (Table S1)**.**

2.3.2. FA functionalized PEBSA/PDA nanoemulsions

FA was added into the PEBSA/PDA emulsion after 3 hours from the reaction start. The samples were left under vigorous stirring (1400 rpm) for 24 hours and were characterized using DLS technique (Table S1)**.**

2.3.3 PTX loaded PEBSA/PDA/FA nanoemulsions

In the case of PEBSA/PDA/FA/PTX nanoemulsions, the same procedure was used. PTX (0.01 g in 0.4 ml sunflower oil) was added, together with retinyl acetate and PEBSA_Brij. After solvation, the oil phase was added dropwise to the Tris-HCl solution. DOPA was then added, and after 3 hours the FA. The resulting nanoemulsions were washed by dialysis with distilled water and characterized using DLS technique (Table S1).

2.4 Nanoemulsion characterization

2.4.1. Physicochemical characterization:

For the determination of the **average hydrodynamic diameter (D_h),** polydispersity index (PDI), and average surface Zeta potential (ζ-pot), DLS measurements were performed using a Malvern Zetasizer Nano ZS90 instrument. For both drug-loaded and unloaded nanoparticles, D_h and PDI values were assessed using a 100 μg/mL dispersion in polystyrene cuvettes. Measurements of the ζ-potential were carried out on the same dispersions placed within folded capillary cells (Malvern Zetasizer Nano series).

The chemical structure of the prepared nanoemulsions and the interactions established between their constituents were studied using **FTIR spectrometry** (Vertex 70, Bruker Germany). Before investigations, 10 μL of the nanoemulsions were spread on KBr disks and then air-dried. Recordings were performed in transmission mode from 4000 to 400 cm^{-1} with a resolution of 4 cm^{-1} and as an average of 64 scans. The spectra were obtained and processed using the OPUS 6.5 software.

Transmission electron microscopy (TEM) was employed to characterize the nanoemulsions morphology. Analyses were performed with the Hitachi High-Tech HT7700 electron microscope from Hitachi High-Tech Corporation, Tokyo, Japan. Micrographs were obtained at an accelerating voltage of 100 kV. Before analysis, nanoemulsions were diluted 50

times with ultrapure water, deposited on carbon-coated copper grids (TED PELLA), and air-dried for 24h.

Fluorescence measurements were recorded at room temperature with a Perkin Elmer fluorescence spectrophotometer. The excitation wavelength was 360 nm, and the emission and excitation slits width were set at 10 and 5 nm. The fluorescence spectra were obtained in the range of 370−700 nm at an integration time of 1.0 s/nm. Optical properties of the prepared nanoemulsion were determined through UV-VIS reflectance spectra measured with the Analytik Jena SPECORD UV-Vis 210Plus spectrophotometer. **UV-VIS spectra** were registered between 230 and 900 nm.

The antioxidant activity of the samples was evaluated by their ability to reduce 2,2-diphenyl-1-picrylhydrazyl (DPPH) radical. The experiments were realised according to the methodology described by da Silva et al. and Brand-Williams et al. [34,35] with slight changes. In the first step, a stock solution of 0.1 mM of DPPH in absolute ethanol was prepared. Subsequently, 0.1 mL of nanoemulsion was put in contact with 3.9 mL of DPPH solution and homogenised. After 90 minutes in a dark place, the colour shift from violet to light yellow was quantified using the UV-VIS spectrophotometer Jenway 6305 (Stone, Staffordshire, UK). Samples UV-VIS absorbance was determined at 515 nm (n=3). DPPH inhibition capacity of the nanoemulsions was calculated using the equation:

$$\text{Inhibition} = \frac{A_c - A_s}{A_c} \times 100 \quad (1)$$

where A_c is the absorbance of the control DPPH solution, and A_s is the absorbance of the DPPH solution containing nanoemulsions.

2.4.2. *In vitro* cytotoxicity

In vitro cytotoxicity of PEBSA/PDA/FA/PTX nanoemulsions was investigated through MTT assay. To perform the *in vitro* cytotoxicity tests, the following reagents, appropriate for cell culture assays, were used: Dulbecco's Modified Eagle Medium – F12 Ham (DMEM/F12 Ham); fetal bovine serum – FBS; antibiotic mixture (penicillin-streptomycin-neomycin mixture - P/S/N, approximately 5,000 units of penicillin, 5 mg of streptomycin, and 10 mg of neomycin per mL, filtered through 0.1 μm); Thiazolyl Blue Tetrazolium Bromide (MTT); Dimethyl Sulfoxide – DMSO. All reagents were acquired from Sigma-Aldrich (Steinheim, Germany).

Initially, human breast adenocarcinoma cells (MCF-7 cell line) were cultured in complete medium consisting of Dulbecco's Modified Eagle's Medium – F12 Ham (DMEM/F12 Ham), supplemented with 10% fetal bovine serum (FBS) and 1% penicillin–streptomycin–neomycin (P/S/N). The cells were then seeded into 96-well plates (50 µL of cell suspension containing 1×10^4 cells in 100 µL DMEM/F12 Ham per well) and incubated for 24 hours at 37°C in a humidified atmosphere with 5% CO_2 to allow cell adherence. Simultaneously, the polymeric delivery systems based on PEBSA_Brij, designed as folic-acid-targeted drug delivery systems and loaded with an antitumoral drug (PTX), were suspended in DMEM/F12 Ham complete medium at concentrations of 0.5, 1, 2.5, and 5 mg/mL. The resulting suspensions were added to the cells and subsequently incubated in a 5% CO_2 atmosphere at 37°C for 24, 48, and 72 hours. Solutions of FA and PTX were also tested for their effects on the cells. Additionally, wells containing cells without the tested suspensions, used as controls, were replenished with fresh medium (DMEM/F12 Ham).

To perform the MTT assay, the suspension solutions were removed from the wells and replaced with MTT working solution (5% MTT in unsupplemented DMEM/F12 culture medium). The cells were incubated with the MTT solution at 37°C for 3 h. Formazan crystals were then solubilized with DMSO (500 µL per well). The absorbance of the resulting purple formazan solution was measured at 570 nm using a Tecan Sunrise plate reader.

The spectrophotometric results obtained from the experimental wells were compared with those from the control wells. Cell viability was calculated by the following equation:

$$\text{Cell viability } (\%) = \frac{\text{Abs}_{\text{sample}}}{\text{Abs}_{\text{control}}} \times 100 \quad (2)$$

Where Abs_{sample} represents the absorbance of the in the well with the nanoemulsion, while $ABS_{control,}$ the absorbance of the control.

The MTT assay was performed at 24, 48, and 72 hours, each in triplicate. To support the MTT results, cell morphology and density were evaluated using an inverted phase-contrast microscope (Leica, Wetzlar, Germany), and images were captured at 10× magnification.

The interaction between PDA and MTT was also evaluated. After the experiment, the absorbance of the PDA-MTT interactions at the tested concentrations was reduced from the initial viability values.

Several live/dead staining assays were performed to evaluate cell morphology. The MCF-7 cell line was cultured with the samples under the same conditions as previously described, in 48-well plates seeded at a density of 8×10^3 cells per well for 72 hours. Cell morphology was assessed using a Calcein AM staining solution, which enables the labelling of live and dead cells. The dye solution, at a concentration of 2 µL/mL, was added to each well and incubated for 30 minutes at 37°C. The second staining assay included DAPI (4,6-diamidino-2-phenylindole) as a fluorescent dye to demonstrate that the cells did not exhibit alterations at the DNA sequence level following exposure to the polymeric suspensions. After a 30-minute formaldehyde fixation step, the cells were permeabilized with 0.1% Triton X-100 at 4 °C for 30 minutes. Subsequently, the cells were washed three times with 1× PBS. The cells were then incubated with a DAPI working solution (1 µL/mL in 0.01 M PBS, pH 7.2) for 30 minutes at 37 °C. The images were obtained using a 10× objective lens from the Leica DM IL LED Inverted Microscope, equipped with a Phase Contrast System and Fluorescence capabilities, manufactured by Leica Microsystems GmbH in Germany.

2.5. Statistical analysis

The experiments were performed in triplicate (n = 3), and the results were expressed as value ± standard deviation (SD). Data were analysed using two-way ANOVA and Tukey's post hoc analysis in order to detect the variables significance and $p < 0.05$ was considered significant.

3. Results and discussions

3.1. Preparation and optimization of PEBSA/PDA nanoemulsions

Because emulsions are less thermodynamically stable, most separate into two phases over time. Their shelf life is limited by droplet aggregation. Therefore, the instability of emulsions can be overcome by reducing the droplet size.

Nanoemulsions are kinetically stabilized systems with improved resistance to phase separation due to reduced droplet size, but even in this case, careful control of parameters is required to achieve a balance between size, stability, and properties. Here, we started from our previous studies in which we obtained an ophthalmic nanoemulsion based on PEBSA_Brij and levofloxacin [33].

In the initial stages, the tests were focused on the PEBSA_Brij variant in which the comonomer ratio was EB/SA = 25/75. For simplicity, and in accordance with Table S1, we will designate this variant with the code $PEBSA_1$. PDA was covered on this $PEBSA_1$ under mild alkaline conditions through an oxidative self-polymerization process to obtain a strong black coating, capable of adhering to the surface of PEBSA (Fig. 1). The introduction of DOPA into the PEBSA-based nanoemulsion system initially induces a tendency for agglomeration. Over time, DOPA transforms into PDA and surrounds the PEBSA_Brij particles, causing interactions between the two polymers that lead to the formation of a monodisperse system after 24 hours (Fig. 2(a)). This stability is maintained even after 8 days of storage. The PDA control fails to maintain its monodispersity over time, and the sample begins to agglomerate after 8 days. The different behavior could be justified, on the one hand, by the existence of interactions between PEBSA_Brij and PDA, evidenced by the zeta potential values. Thus, in the case of the $PEBSA_1$/PDA sample (−25.7 mV), the values are different from those of PDA (−25 mV) and $PEBSA_1$ (−41.5 mV). On the other hand, the main driving force in the case of the PEBSA-PDA complex is represented by the adhesion force of PDA, which predominantly forms the final complex.

To achieve the optimal nanoemulsion formulation, the influence of the surfactant, oil concentration, and PEBSA/PDA ratio on the particle stability and size was studied (Fig. 1(A)). To obtain a more stable emulsion, the surfactant content was varied between 0.1% and 0.6% (Fig. S1(a)).

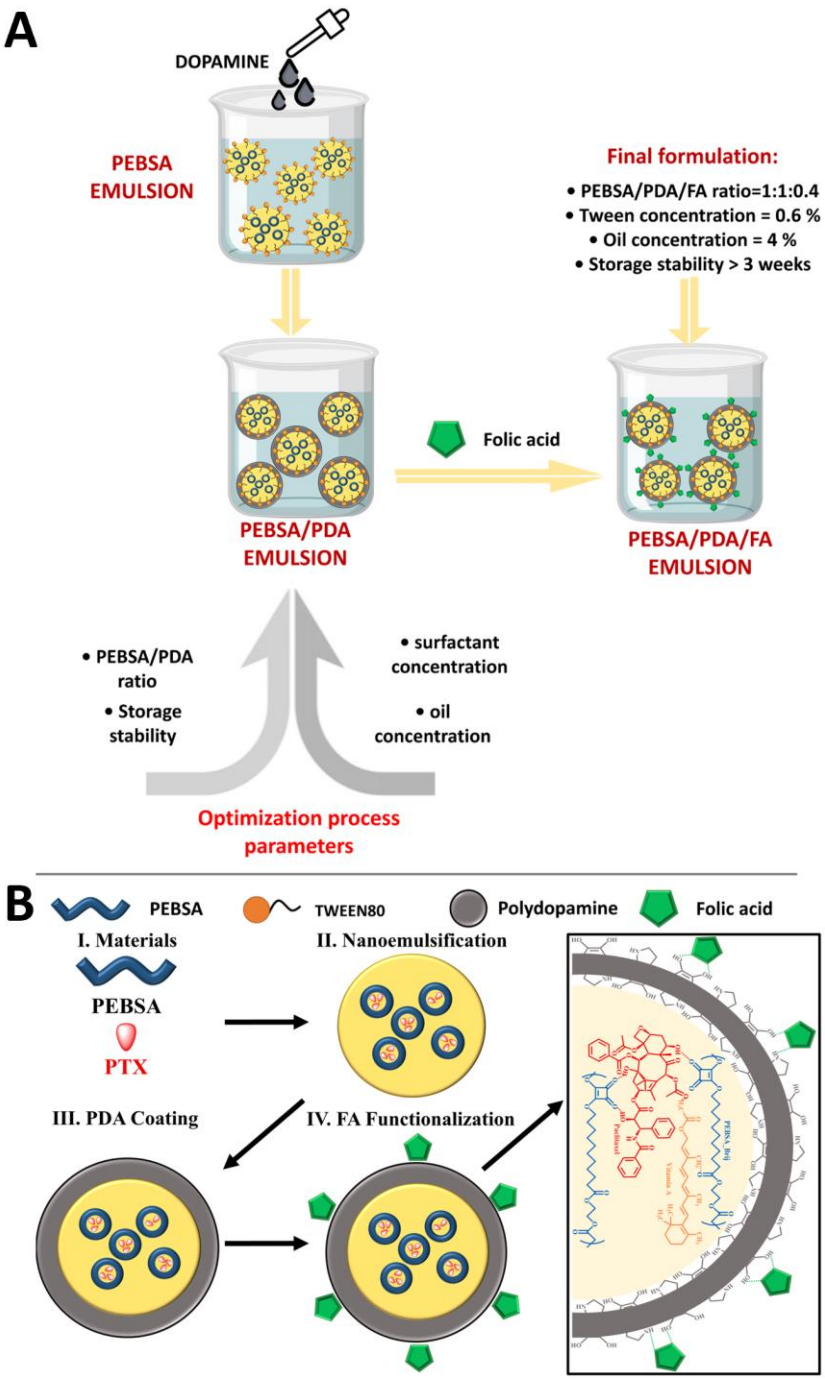

Fig. 1(A) Schematic representation of PEBSA/PDA/FA nanoemulsion formation; (B) Schematic representation of PEBSA/PDA/FA/PTX nanoemulsion formation.

The surfactant reduces the interfacial tension between the phases. This prevents the possibility of coalescence and preserves kinetic stability. Particle aggregation occurs at both low and high surfactant concentrations. At low surfactant content, aggregation can be attributed to

incomplete surface coverage, resulting in insufficient electrostatic or steric stabilization. Increasing the concentration above the critical micelle concentration also leads to aggregation due to shielding effects and interactions with the surfactant. These competing effects led us to establish that 0.6% Tween 80 concentration to be better for obtain monodisperse samples with a size of approximately 190 nm. Therefore, this surfactant concentration was used in subsequent studies. Regarding the influence of the oil concentration, three concentrations were used from 1wt% to 4wt%. It was detected that a lower oil concentration causes a destabilization of the emulsion. For these reasons, the oil concentration was kept constant throughout the experiment 4%.

The choice of the PEBSA/PDA ratio was of particular importance in the next stage of the study. Thus, a higher amount of PDA may increase the amount of FA entrapped, with positive influences on targeting malignant tissue, but can decrease the stability of the nanoemulsion. By studying three mass ratios between PEBSA_Brij and PDA, respectively 1:2, 1:1, and 2:1, it was found that the 1:1 ratio is the most feasible, the resulting emulsion maintaining its stability even after 3 weeks (Fig. 2(a), S1(b) and S1(c)). The zeta potential value, which in the 1:1 ratio has the lowest modulus value (−25.7 mV) in comparison to −24 mV (PEBSA/PDA=2:1) and −27.8 mV (PEBSA/PDA=1:2), can also be linked to this behavior. This indicates that the 1:1 ratio promotes strong interactions between the two polymers. Additionally, the dimensions rise with increasing PDA amount from 178 nm (PEBSA/PDA=2:1) to 182 nm (1:1 ratio) and 267 nm (in the case of 1:2 ratio), respectively.

In conclusion, following all tests, the optimal process conditions for the preparation of nanoemulsions were obtained, as follows: PEBSA/PDA=1:1, surfactant concentration: 0.6% by weight, oil phase concentration 4% (Fig. 1).

As expected, the increase in the content of the long-chain, large-molecule hydrophobic monomer (EB) causes a considerable increase in the particle size from 182 nm ($PEBSA_1$/PDA) to 251 nm ($PEBSA_3$/PDA) – Fig. S1(d). It is worth noting that, in the case of $PEBSA_1$ and $PEBSA_2$, the presence of PDA determines a decrease in the particle size (Table S1), which shows that in this circumstance the interactions are stronger due to the presence of a larger amount of squaric acid and, implicitly a larger number of functional groups.

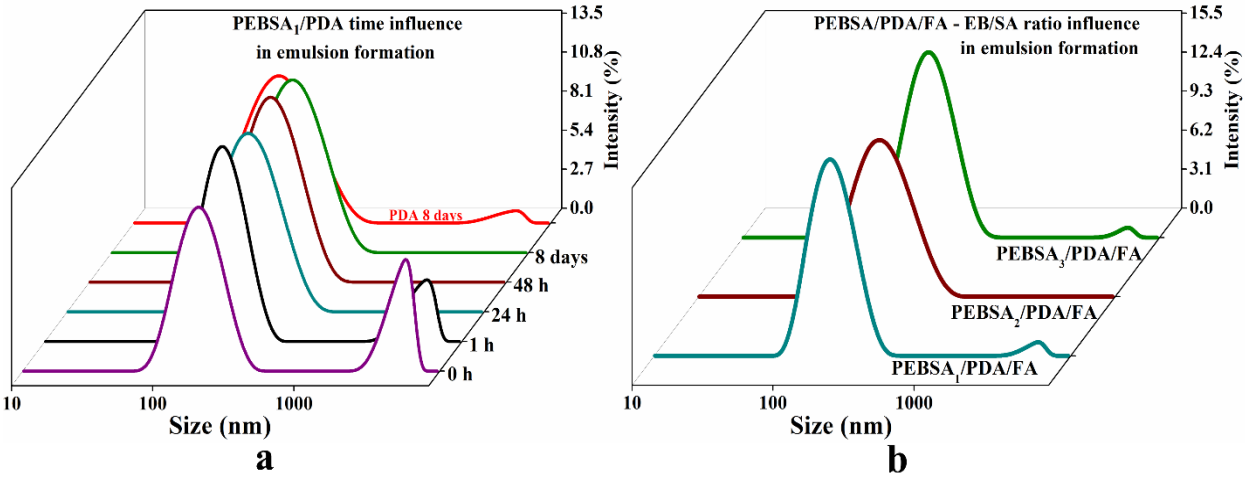

Fig. 2. DLS studies: a) $PEBSA_1$/PDA nanoemulsion-stability in time; b) EB/SA ratio influence onto emulsion formation

3.2. Preparation of FA functionalized PEBSA/PDA nanoemulsions

As already mentioned, PEBSA/PDA nanoemulsions are prepared by oxidative polymerization of dopamine hydrochloride with the formation of a PDA shell around the PEBSA_Brij core. PEBSA/PDA/FA was obtained by physical adsorption of FA onto the PEBSA/PDA to prevent a premature release of drugs to non-target organs as well as achieving site-specific targeting to cancer cells. The addition of FA (Fig. 2(b)) does not considerably modify the particle size, except for $PEBSA_3$, where a decrease in diameter by 40 nm occurs (Table S1), but even in this case, the diameters of the $PEBSA_3$-nanoemulsions are the highest. The zeta potential modulus decreased when the FA is added with about 30% (except $PEPSA_3$), which attests the covering of the particles with FA [36,37]. Moreover, this fall in ZP modulus can be caused owing to interactions of FA with the charged groups on the PDA surface. The ability of FA to influence the aggregate structure of self-polymerized dopamine was an unexpected result that was demonstrated in previous works [38]. FA is composed of pterin (PT), p-aminobenzoic acid, and glutamic acid moieties. The PT ring is an N-planar heterocycle, which can act as a π acceptor to interact with strong π donors, such as polycyclic aromatic hydrocarbons and polythiophene derivatives [39]. The combination of π–π interactions and hydrogen bonds allows the formation of ordered supramolecular structures. Since π–π interactions are known supramolecular interactions tangled in the assembling of melanin protomolecules, the ability of FA to interact with PDA-coated nanoemulsions may stem in part from its role as a π acceptor.

3.3. Preparation of PEBSA/PDA/FA/PTX nanoemulsions

As a natural biopolymer, PDA is rich in reductive functional groups consisting of catechol and imine. As a result, PDA exhibits prominent capabilities to scavenge various radical species, such as ROS, as well as to reduce ROS-induced inflammation. Therefore, PDA-modified nanoparticles may be a promising candidate as a radical scavenger for anti-inflammatory and antitumor treatment. There are certain types of drugs that have the ability to self-assemble. These self-assembling drug cores, for example, doxorubicin nanoparticles, PTX nanoparticles, and tanshinone IIA nanoparticles, can be coated with PDA to prolong the blood circulation time as well as to prevent the pre-leakage of the cargo. More importantly, the thiolate and quinone groups on PDA can interact with the FA groups, while the drug, due to the core/shell self-assembly mechanism, is inside. In this study, PTX was selected as a model antitumor drug and was loaded during the nanoemulsion formation process (Fig. 1(B)), considering the proven ability of PEBSA_Brij to incorporate hydrophobic compounds. The introduction of PTX causes a slight increase in particle size, as expected, but also a decrease in the zeta potential modulus (Table S1), which shows the occurrence of physical interactions between PTX, PDA, and FA.

3.4. Morphological characterization

The morphology of the nanomicelles was investigated by TEM (Fig. 3). As shown in Fig. 3, the nanomicelles were spherical and exhibited a smooth surface. The $PEBSA_1$/PDA/FA/PTX and $PEBSA_3$/PDA/FA/PTX samples show the same morphology (for example, the $PEBSA_1$/PDA/FA/PTX sample is shown in Fig. 3(a)) with well-defined particles with moderate contrast, suggesting a compact structure with good encapsulation of PTX. The $PEBSA_2$/PDA/FA/PTX (Fig. 3(b)) sample shows a different morphology. It seems that the stoichiometric ratio between EB and SA determines the formation of structures with sharp peripheral contrast, which shows a better functionalization with PDA and FA, confirming the success of obtaining a well-defined nanostructured system suitable for targeted delivery of PTX.

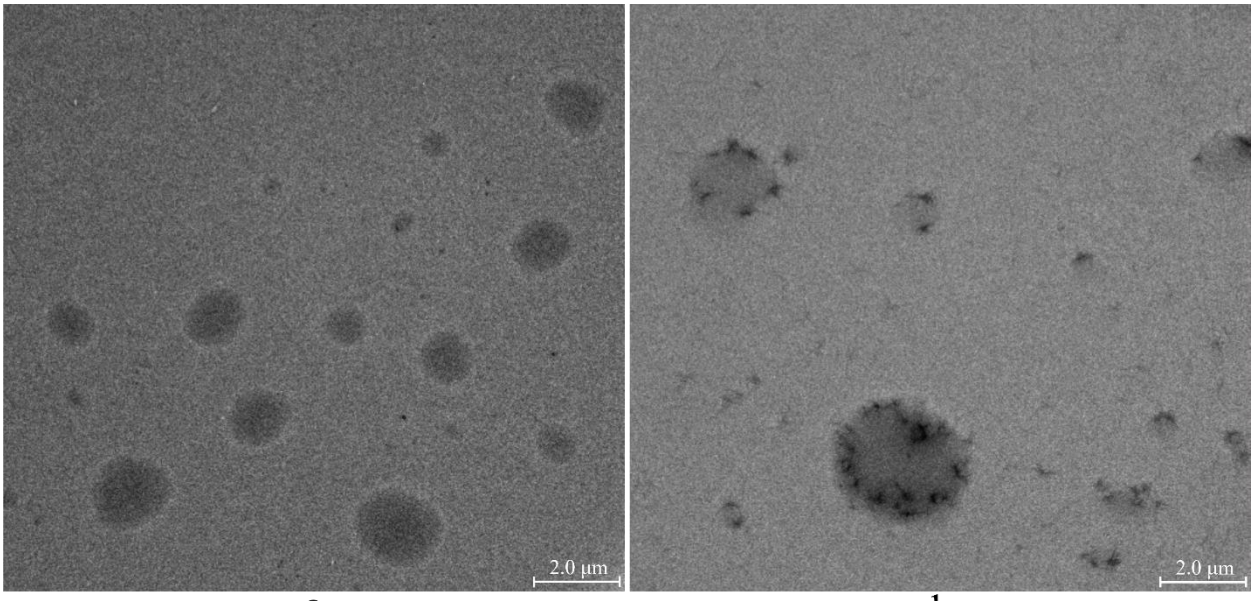

Fig. 3. TEM of $PEBSA_1$/PDA/FA/PTX (a) and $PEBSA_2$/PDA/FA/PTX (b).

3.5. FTIR Characterization

Fig. 4.(a), and (b) illustrate comparative FTIR spectra of pristine and PTX-loaded nanoemulsions. Aditionally FTIR spectra of nanoemulsion constituents are illustrated in Fig. S2(a), Supporting Information.

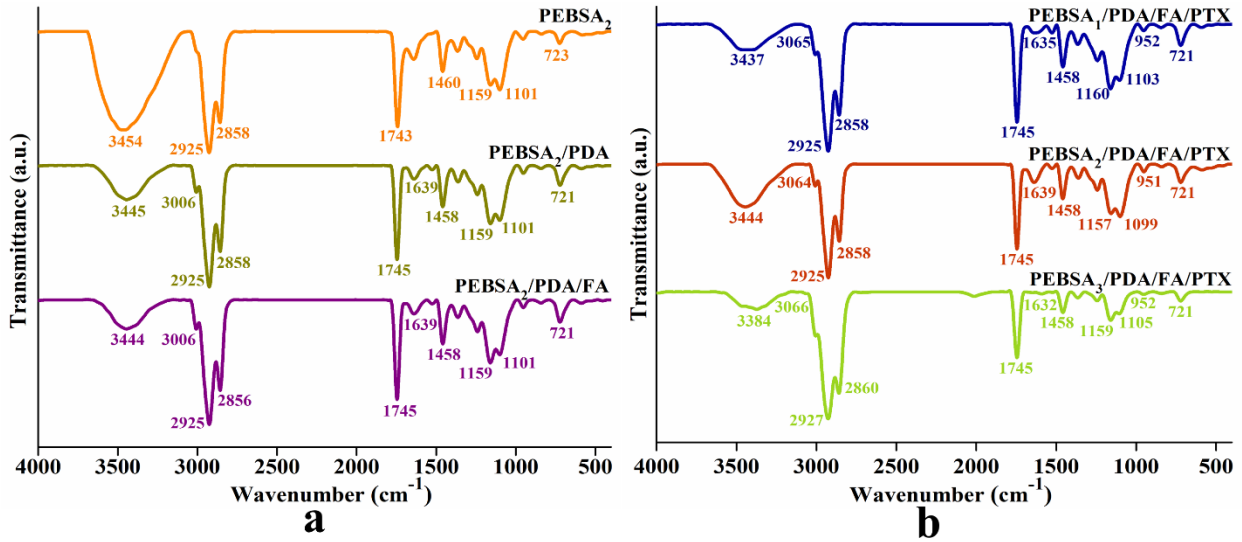

Fig. 4. FITR spectra $PEBSA_2$-nanoemulsions (a), and PTX-loaded nanoemulsions (b).

The FTIR bands identified in the spectrum of the pure nanoemulsion, $PEBSA_2$, correspond mainly to its constituents: vitamin A, $PEBSA_{50/50}$_Brij, and Tween 80 [30,40,41].

The most important bands are associated with: C−H_2 stretching and bending vibrations (2925, 2858, and 1460 cm^{-1}); C=O stretching vibration, 1743 cm^{-1}; C−O stretching vibration (1243, 1101 cm^{-1}), and C−O−C 1159 cm^{-1}stretching vibration. The wide band from 3454 cm^{-1} is characteristic for the stretching vibration of O−H functional groups from the Tween 80 and residual water. The presence of water molecules can also be attested through the shoulder-like band from 1642 cm^{-1}.

The PDA coating of the nanoemulsion droplets is confirmed by the spectral changes observed between 3500−3000 cm^{-1} and 1700−1500 $cm^{-1,}$ respectively (Fig. 4(a)). The reduction in intensity and the shift to lower wavenumbers of the bands specific to the O−H and N−H stretching vibration, observed through parallel analysis of PDA (Fig. S2(a)) and $PEBSA_2$ spectra, confirms the formation of hydrogen bonds between the constituents of the primary emulsion and the polymeric layer. The PDA structure is also confirmed by the appearance of two new bands at 1525 and 3006 cm^{-1} in the spectrum of $PEBSA_2$/PDA, corresponding to the bending vibration of N−H and stretching vibration of C−H from the aromatic moieties [42,43]. Additionally, a well-defined band appears at 1639 cm^{-1}, corresponding to aromatic C=C stretching vibration [44].

Comparative analysis of the FTIR spectra of FA (Fig. S2(a)) and $PEBSA_2$/DOPA/FA confirms the surface modification of the droplets and the physical nature of the bonds that are established. The functional groups, phenyl, carboxyl, amine, or amide, of FA and PDA facilitate the formation of hydrogen, electrostatic, and π−π bonds that lead to the functionalization of the nanomicelles surface. The successful formation of hydrogen bonds is attested by the reduction of the intensity of the band assigned to stretching vibrations of the O−H bonds found at 3444 cm^{-1}. The slight increase in the intensity of bands registered at 1745, 1639, and 1525 cm^{-1} highlights the presence of carboxyl and amide functional groups belonging to FA molecules [45].

PTX FTIR characteristic features include the bands assigned to: O−H and N−H stretching vibration (3479 cm^{-1}), C−H and C−H_2 asymmetric and symmetric stretching vibration (3066, 2947 and 2887 cm^{-1}), C=O stretching vibration of the ester groups (1724 cm^{-1}) and of the amide groups (1647 cm^{-1}), N−H bending and C−N stretching vibration (1531 cm^{-1}), C−O stretching vibration (1252 and 1070 cm^{-1}), and aromatic C−H bending (707 cm^{-1}) [46,47].

The successful encapsulation of PTX inside nanoemulsion droplets is attested by a new, low-intensity band at ~3065, specific to the stretching vibrations of the aromatic C−H bonds, and by the increase in the intensity of the aromatic C−H bending band at 721 cm^{-1}. No other PTX-

specific bands were identified in the FTIR spectrum, mainly due to the structural similarities between the model drug and the constituents of the nanoemulsion droplets. The establishment of physical bonds, and especially hydrogen bonds, between vitamin A, PEBSA_Brij, or PDA and PTX is highlighted by the reduction in the intensity and the shift to lower wavelengths of bands assigned to the functional groups involved, namely hydroxyl, amino, amido, and carboxyl.

3.6. Optical properties

The optical properties of PEBSA/PDA/FA/PTX were analyzed. From the UV-VIS absorption spectra showed in Fig. 5, we can see that two characteristic peaks appear at about 252 and 333 nm, corresponding to the π-π* electronic transitions of the C=C, and n-π* electronic transitions of C=O/C=N, respectively. The decrease in the intensity of $PEBSA_2$/PDA/FA/PTX below that of the $PEBSA_2$/PDA and $PEBSA_2$/PDA/FA samples shows that the electrostatic interaction that occurs between the compounds facilitates the formation of the complex. This observation is in agreement with the specialized literature [48,49].

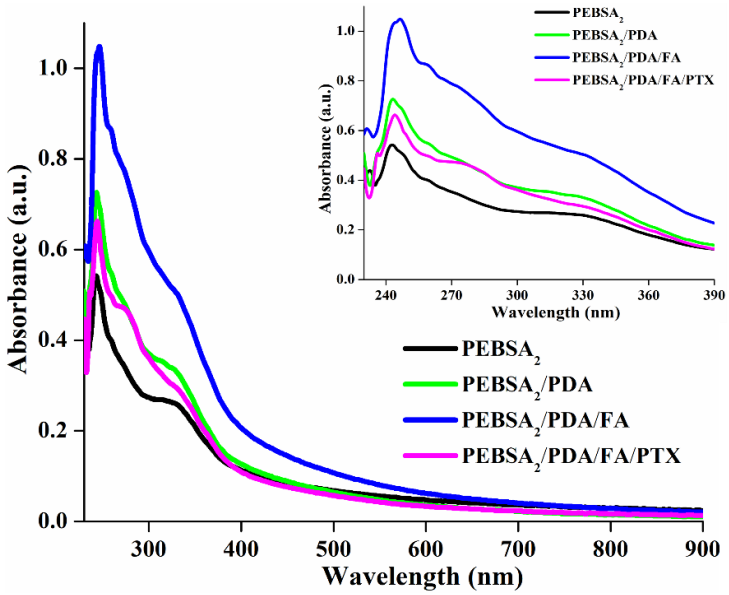

Fig. 5. UV-Vis spectra of $PEBSA_2$/PDA/FA/PTX compared with its precursors

The fluorescence spectra presented in Fig. 6 and Fig. S3(a), (b), (c) show a predominantly blue emission, with a well-defined maximum located around 460–470 nm. This emission is characteristic of electronic transitions in the conjugated systems of the polymer matrix and the aromatic groups present in the structure. The relative intensity of the fluorescent signal varies

significantly between samples, with a progressive decrease in intensity observed with successive functionalization of the material.

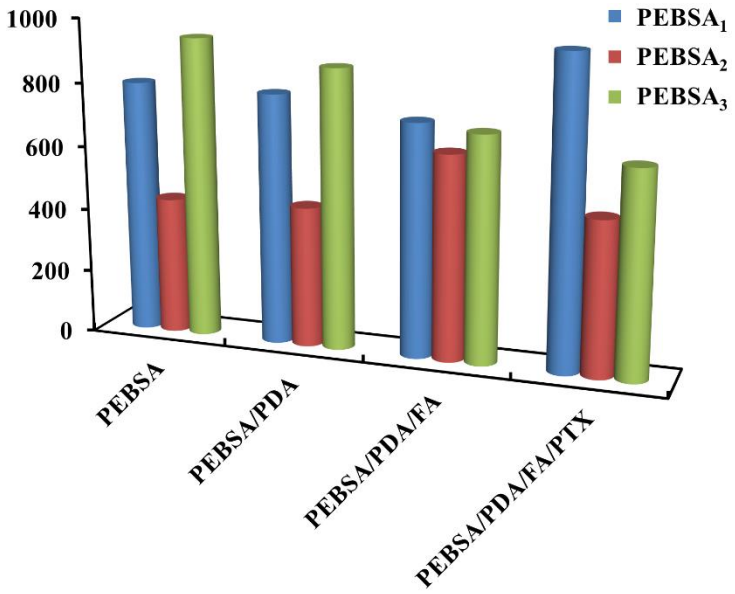

Fig. 6. Fluorescence spectra comparison between PEBSA_Brij with different molar ratio between components (excitation wavelength is 360 nm).

The fluorescence spectra of PEBSA_Brij have been studied and published previously [50] and showed a dependence of the fluorescence intensity on the molar ratio of the EB/SA comonomers. Thus, a significant fluorescence quenching is recorded in the case of the equimolar ratio of 50/50 (Fig. S3(b)), which can be attributed to the increased inter-chain self-assembly with carbonyl groups oriented inside the polymer particle, an aspect also supported by the literature [32]. The physical interactions between the EB and SA segments, which lead to the formation of self-assembled chains, are also sustained by the DLS results that indicated a decrease in the hydrodynamic radius (R_H) of the polymer particles at the stoichiometric ratio of the comonomers (Fig. 2 and S1).

The introduction of dopamine (PDA) causes a reduction in fluorescence intensity, which can be attributed to the quenching effect produced by the catechol groups, π-π stacking interaction between the oligomeric units in PDA [51,52]. These can interact with the excited states of the fluorophores through electron transfer mechanisms or by the formation of exciplex complexes, thus reducing the quantum yield of the emission. The addition of FA accentuates the decrease in intensity, suggesting the occurrence of additional interactions between the chromophore moieties of FA and the conjugated polymer system [53]. Their presence, including

PTX (except PEBSA$_1$/PDA/FA/PTX), leads to a decrease in emission efficiency but without a significant shift in the maximum wavelength, suggesting the preservation of the initial fluorescent core with the impairment of radiative recombination efficiency through intermolecular interactions and possible aggregation effects.

3.7. Antioxidant activity

All samples shown considerable antioxidant activity, above 85% (Fig. 7), indicating a strong antioxidant activity of the nanoemulsions systems. The antioxidant behavior of the compounds is influenced by the PEBSA_Brij composition, thus a higher amount of squaric acid causes an increase in the antioxidant character attributed to the carbonyl groups of squaric acid present in the structure of the copolymacrolactone. The specialized literature also mentions the antioxidant character of compounds containing squaric acid due to their strong electron donating character [32]. The presence of FA increases the antioxidant capacity of the nanoemulsions. The antioxidant activity of FA is mediated by multiple mechanisms, including a reduction in plasma HCY concentrations, which can increase the total antioxidant capacity and reduce the formation of ROS.

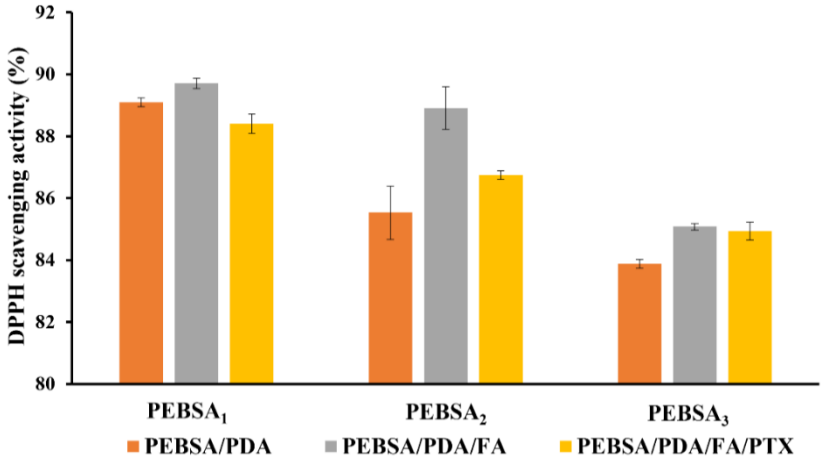

Fig. 7. Antioxidant activity of samples.

In the context of antitumor therapy, the presence of antioxidant activity may provide a dual functionality: (i) protection of non-malignant cells against oxidative damage and (ii) modulation of oxidative stress in the tumor microenvironment, potentially contributing to cytoprotective effects in non-malignant cells and modulating oxidative stress-related side effects and biocompatibility. Although antioxidants are traditionally considered protective, their role in

cancer therapy is context-dependent. Many effective chemotherapeutic agents work by inducing massive ROS generation that exceeds the threshold of tumor cells, leading to apoptosis. But, a sustained antioxidant activity of the obtained nanoemulsions is justified by protecting healthy tissues from the inevitable oxidative damage caused by the loaded anticancer agent as well as to attenuate chemotherapy-induced toxicity. Also, reducing chronic inflammation (mediated by ROS) in the tumor microenvironment can inhibit cancer progression and angiogenesis. Thus, the observed antioxidant activity acts as a protective adjuvant, rather than an inhibitor of tumor-directed ROS, ultimately seeking to improve the therapeutic index rather than compromising the efficacy of the cargo [54,55]. Therefore, the developed nanoemoulsions system exhibits not only antitumor and targeting properties but also intrinsic antioxidant functionality, highlighting its multifunctional therapeutic potential.

3.8. *In vitro* cytotoxicity assays

The study aimed to obtain and characterize different types of PEBSA/PDA/FA/PTX-based nanoemulsions. During the characterization of their properties, their antitumoral activity was analyzed on human breast adenocarcinoma cells (MCF-7 cell line). Cytotoxicity was assessed using tumoral cell cultures via the MTT assay. This approach is a standard method for examining biological responses (ISO 10993-5) and for evaluating the influence of polymer nanoemulsions on cell viability compared to control cell cultures [56,57]. The results are presented in Fig. 8(a) and (b). The PEBSA/PDA/FA-based nanoemulsions maintained cell viability above 90%, as assessed by mitochondrial dehydrogenase activity. Cells treated with drug-free polymer samples, regardless of concentration, also exhibited good viability (approximately 80% at 24 h), which slightly decreased due to the addition of surfactant during nanoemulsion synthesis.

In contrast, cells treated with PTX-loaded polymer systems exhibited a pronounced reduction in viability, decreasing to <70% after 72 h of incubation. The difference between the control polymer and PTX-loaded formulations became more pronounced over time, indicating a sustained cytotoxic effect. These results suggest that the observed reduction in cell viability is primarily attributable to PTX release from the polymer systems.

PTX and PEBSA/PDA/FA/PTX nanoemulsions with different EB/SA ratios were evaluated for cytotoxicity at different concentrations (0.5–5 mg/mL) and incubation times (24, 48 and 72 h)

(Fig. 8(b)).At lower concentrations (0.5–1 mg/mL), all formulations showed moderate cytotoxicity, with cell viability remaining above 60%. In contrast, higher concentrations (2.5–5 mg/mL) led to a marked reduction in cell viability, particularly after 72 h of exposure. This progressive decrease suggests that extended exposure enhances intracellular drug activity and apoptotic response, indicating a time-dependent therapeutic effect.

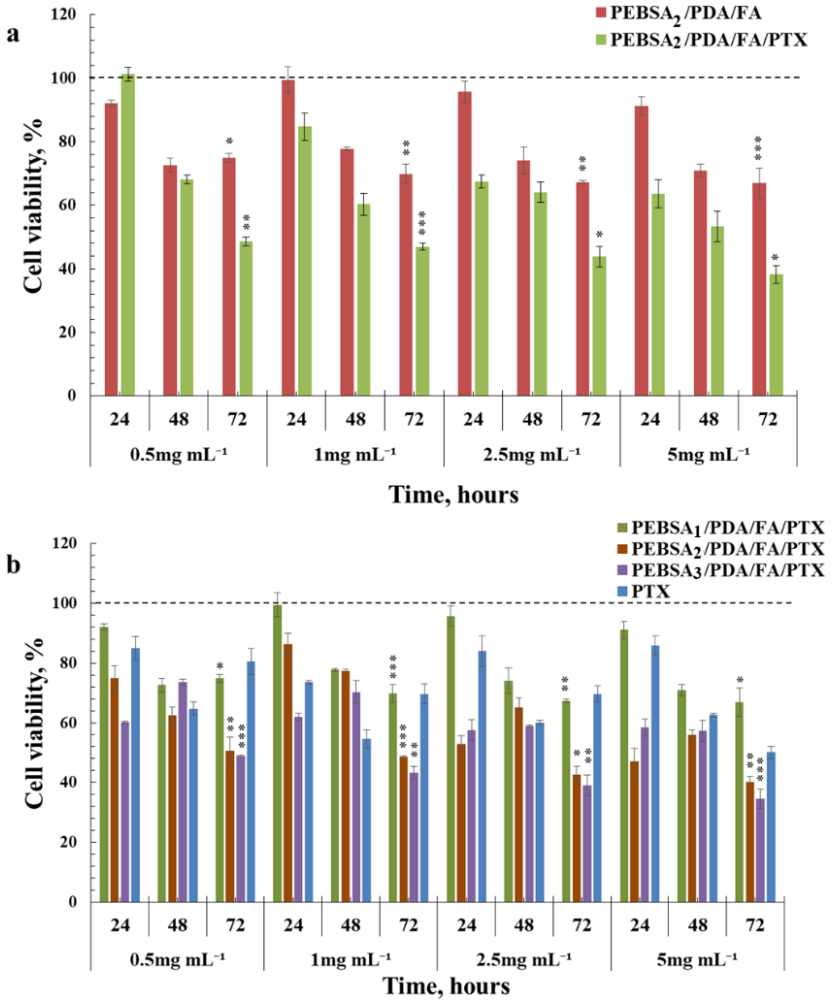

Fig. 8.(a) Cell viability data from the MTT assays for $PEBSA_2$/PDA/FA compared with $PEBSA_2$/PDA/FA/PTX; (b) Influence of EB/SA ratio and PTX into PEBSA/PDA/FA/PTX samples tested on human breast adenocarcinoma cells (MCF-7 cell line). Data are expressed as the means ± SD of three experiments; *$p < 0.05$, **$p < 0.01$, ***$p < 0.001$ versus control (free cell culture).

The cytotoxic activity of PTX and PEBSA/PDA/FA/PTX nanoemulsions with varying EB/SA ratios (25/75, 50/50, 75/25) was investigated at concentrations ranging from 0.5–5 mg/mL over incubation times of 24, 48, and 72 h (Fig. 8(b)). All PTX-loaded formulations

exhibited clear dose- and time-dependent cytotoxicity, consistent with PTX's established mechanism of mitotic arrest and apoptosis. At 24 h, $PEBSA_1$/PDA/FA/PTX (25/75) demonstrated the most rapid onset of cytotoxicity, with cell viability decreasing to approximately 90% at 5 mg/mL. This accelerated activity is attributed to the higher squaric acid content, which enhances hydrophilicity and facilitates cellular interactions and drug release. $PEBSA_3$/PDA/FA/PTX (75/25) showed moderate initial activity, while $PEBSA_2$/PDA/FA/PTX (50/50) exhibited a gradual cytotoxicity profile at this early time point.

By 72 h, the therapeutic hierarchy had shifted. $PEBSA_3$/PDA/FA/PTX exhibited the lowest cell viability values (< 30% at 5 mg/mL), indicating an enhanced therapeutic effect. $PEBSA_1$/PDA/FA/PTX showed comparable final cytotoxicity but a less pronounced dose-dependent trend, suggesting an initial burst release followed by depletion of the drug reservoir. $PEBSA_2$/PDA/FA/PTX maintained intermediate activity, likely reflecting more controlled release kinetics associated with its hydrophobic core.

These temporal differences reveal distinct release profiles: $PEBSA_1$ provides rapid drug availability, $PEBSA_3$ offers prolonged retention, and $PEBSA_2$ achieves the optimal balance of effective folate receptor-mediated uptake, controlled PTX release, and sustained intracellular drug concentration. The equimolar EB/SA ratio in $PEBSA_2$ promotes optimal self-assembly and surface functionalization, as evidenced by its well-defined morphology (Fig. 3(b)) and intermediate particle size (174 nm), facilitating efficient receptor-mediated endocytosis.

The FR is a cell surface glycoprotein involved in the recognition and internalization of FA, an essential nutrient required for DNA synthesis and cell proliferation. The breast cancer cell line MCF-7 is known to express folate receptors and is therefore widely used as a relevant model for evaluating targeted FA-based drug delivery systems [58]. Functionalization of the PEBSA/PDA nanoemulsions with FA allows specific interaction with FR and promotes receptor-mediated endocytosis, thereby facilitating intracellular delivery of PTX. The differences registered between the three nanoemulsions in terms of cell viability and morphological changes suggest variations in the efficiency of FR-mediated uptake as well as in the kinetics of PTX release. The $PEBSA_1$/PDA/FA/PTX nanoemulsion induces a cytotoxic effect at 72h accompanied by a significant reduction in cell confluence and nuclear density, possibly due to FR-mediated internalization and enhanced intracellular release of PTX. The $PEBSA_3$/PDA/FA/PTX nanoemulsion exhibits an intermediate effect, characterized by moderate

morphological changes and relatively higher cell viability, suggesting a more controlled release profile. In contrast, the PEBSA$_2$/PDA/FA/PTX nanoemulsion maintains the highest cell viability and exhibits morphology comparable to the control, indicating reduced interaction with FR and/or a slower release of PTX, which limits intracellular drug exposure. Overall, these observations highlight the critical role of FR-mediated targeting, in synergy with the nanoemulsion composition, in modulating the therapeutic efficacy of PTX-loaded delivery systems in MCF-7 breast cancer cells (Fig. 9 and S4).

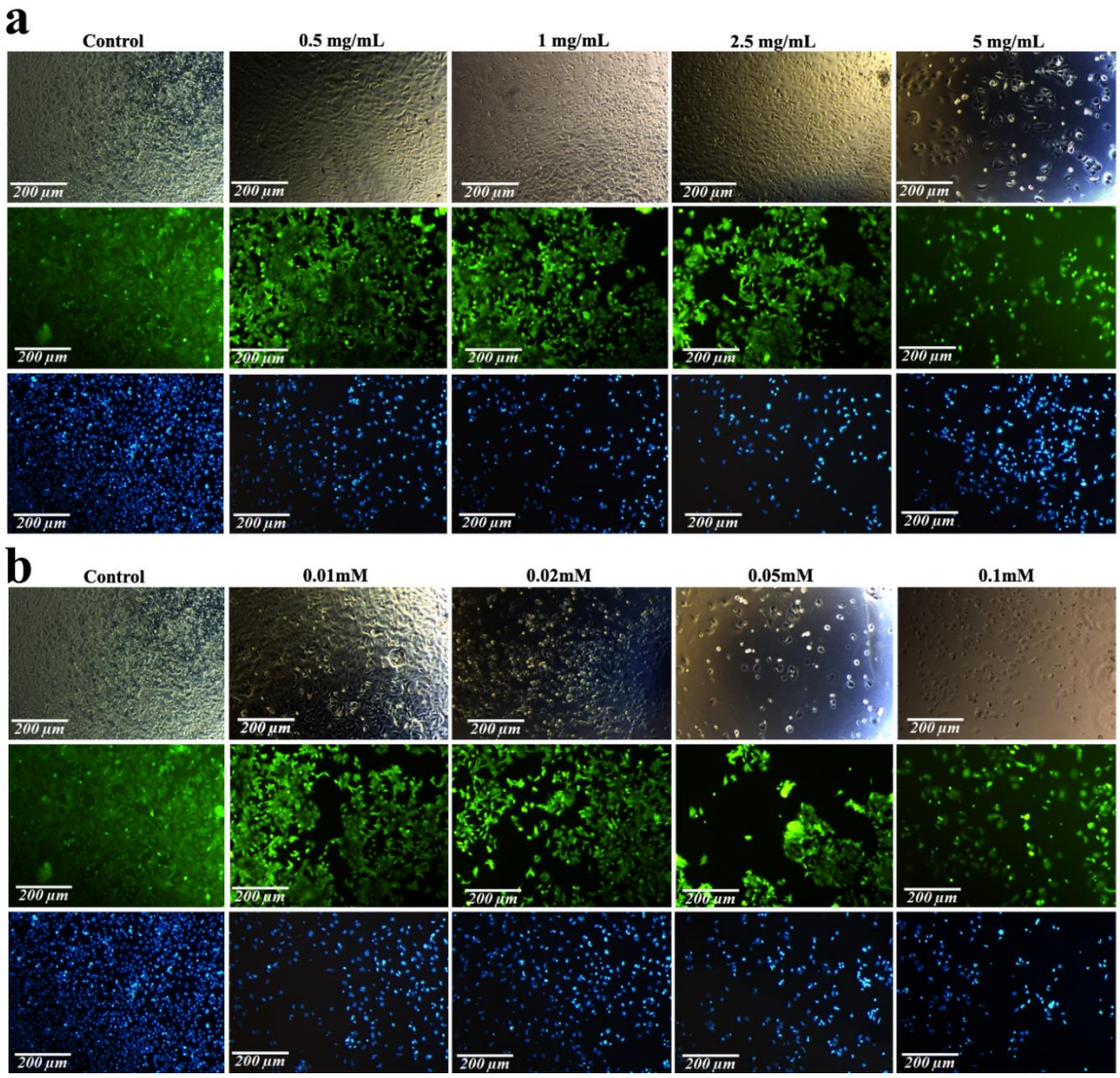

Fig. 9. Cell morphology after direct contact with a) PEBSA$_3$/PDA/FA/PTX and b) free PTX.

Quantitative viability data obtained at 24, 48, and 72 h reveal a clear nanoemulsion and dose-dependent response in MCF-7 breast cancer cells, and the data are supported by the

corresponding morphological observations. At 24 h, $PEBSA_1$/PDA/FA/PTX already induces measurable cytotoxicity at higher concentrations, with morphological images showing early reduction in cell confluence and altered cellular organization. These effects reflect rapid folate receptor uptake and initial intracellular PTX release facilitated by high squaric acid content. By 48 and 72 h, $PEBSA_2$/PDA/FA/PTX exhibits the lowest viability values across all concentrations, accompanied by severe morphological changes, including extensive loss of adherent cells and decreased nuclear density. This demonstrates optimal folate receptor-mediated internalization combined with sustained intracellular drug exposure. $PEBSA_3$/PDA/FA/PTX shows intermediate time- and dose-dependent cytotoxicity, with partially preserved cell attachment and heterogeneous nuclear distribution, suggesting more controlled but more efficient receptor-mediated uptake compared to $PEBSA_2$. The morphological analysis confirms these quantitative trends: $PEBSA_2$/PDA/FA/PTX induces the most pronounced cellular damage, while $PEBSA_3$ maintains better-preserved morphology at equivalent drug concentrations.

4. Conclusion

In conclusion, PTX-loaded polymeric nanoparticles functionalized with FA were successfully developed with dimensions ranging from 170–181 nm depending on PEBSA_Brij composition. The homogeneity of the obtained particles was demonstrated by DLS and TEM. Comparative evaluation in MCF-7 breast cancer cells revealed formulation-dependent cytotoxicity profiles directly correlated with EB/SA ratio-dependent drug release kinetics and folate receptor-mediated uptake efficiency.

$PEBSA_2$/PDA/FA/PTX (50/50 EB/SA) exhibited the highest overall therapeutic efficacy, achieving maximal cytotoxicity at 72 h with well-balanced drug release and optimal surface functionalization for receptor targeting. $PEBSA_1$/PDA/FA/PTX (25/75) demonstrated rapid initial activity suitable for applications requiring fast drug availability, while $PEBSA_3$/PDA/FA/PTX (75/25) provided more sustained but less pronounced cytotoxic effects.

These findings highlight the critical importance of polymer composition in modulating nanocarrier performance and validate the rational design of EB/SA 50/50 as the optimal formulation for targeted breast cancer therapy. The obtained results support further optimization and *in vivo* evaluation of this multifunctional delivery platform.

Acknowledges: This research is carried out and financed within the framework of the second Swiss Contribution MAPS (project code: F-RO-CH-2024-0081)

References

[1] M. Zhou, S. Han, O. Aras, F. An, Recent Advances in Paclitaxel-based Self-Delivery Nanomedicine for Cancer Therapy, Curr. Med. Chem. 28 (2021) 6358–6374. https://doi.org/10.2174/0929867327666201111143725.

[2] H.A. Abouzeid, L. Kassem, X. Liu, A. Abuelhana, Paclitaxel resistance in breast cancer: Current challenges and recent advanced therapeutic strategies, Cancer Treat. Res. Commun. 43 (2025) 100918. https://doi.org/10.1016/j.ctarc.2025.100918.

[3] D. Peer, J.M. Karp, S. Hong, O.C. Farokhzad, R. Margalit, R. Langer, Nanocarriers as an emerging platform for cancer therapy, Nat. Nanotechnol. 2 (2007) 751–760. https://doi.org/10.1038/nnano.2007.387.

[4] N. Ying, S. Liu, M. Zhang, J. Cheng, L. Luo, J. Jiang, G. Shi, S. Wu, J. Ji, H. Su, H. Pan, D. Zeng, Nano delivery system for paclitaxel: Recent advances in cancer theranostics, Colloids Surf. B Biointerfaces. 228 (2023) 113419. https://doi.org/10.1016/j.colsurfb.2023.113419.

[5] J. Shi, P.W. Kantoff, R. Wooster, O.C. Farokhzad, Cancer nanomedicine: progress, challenges and opportunities, Nat. Rev. Cancer 17 (2017) 20–37. https://doi.org/10.1038/nrc.2016.108.

[6] P. Ma, R.J. Mumper, Paclitaxel Nano-Delivery Systems: A Comprehensive Review, J. Nanomed. Nanotechnol. 4 (2013) 1000164. https://doi.org/10.4172/2157-7439.1000164.

[7] N. Kamaly, B. Yameen, J. Wu, O.C. Farokhzad, Degradable Controlled-Release Polymers and Polymeric Nanoparticles: Mechanisms of Controlling Drug Release, Chem. Rev. 116 (2016) 2602–2663. https://doi.org/10.1021/acs.chemrev.5b00346.

[8] H.K. Makadia, S.J. Siegel, Poly Lactic-co-Glycolic Acid (PLGA) as Biodegradable Controlled Drug Delivery Carrier, Polymers 3 (2011) 1377–1397. https://doi.org/10.3390/polym3031377.

[9] S. Sur, A. Rathore, V. Dave, K.R. Reddy, R.S. Chouhan, V. Sadhu, Recent developments in functionalized polymer nanoparticles for efficient drug delivery system, Nano-Struct. Nano-Objects. 20 (2019) 100397. https://doi.org/10.1016/j.nanoso.2019.100397.

[10] F. Wang, M. Porter, A. Konstantopoulos, P. Zhang, H. Cui, Preclinical development of drug delivery systems for paclitaxel-based cancer chemotherapy, J. Control. Release. 267 (2017) 100–118. https://doi.org/10.1016/j.jconrel.2017.09.026.

[11] X.-H. Tang, L.J. Gudas, Retinoids, Retinoic Acid Receptors, and Cancer, Annu. Rev. Pathol. Mech. Dis. 6 (2011) 345–364. https://doi.org/10.1146/annurev-pathol-011110-130303.

[12] L. Altucci, H. Gronemeyer, The promise of retinoids to fight against cancer, Nat. Rev. Cancer 1 (2001) 181–193. https://doi.org/10.1038/35106036.

[13] G.-Y. Hong, Y.-I. Jeong, S.J. Lee, E. Lee, J.S. Oh, H.C. Lee, Combination of paclitaxel- and retinoic acid-incorporated nanoparticles for the treatment of CT-26 colon carcinoma, Arch. Pharm. Res. 34 (2011) 407–417. https://doi.org/10.1007/s12272-011-0308-8.

[14] R. Sun, Y. Liu, S.-Y. Li, S. Shen, X.-J. Du, C.-F. Xu, Z.-T. Cao, Y. Bao, Y.-H. Zhu, Y.-P. Li, X.-Z. Yang, J. Wang, Co-delivery of all-trans-retinoic acid and doxorubicin for cancer therapy with synergistic inhibition of cancer stem cells, Biomater. 37 (2015) 405–414. https://doi.org/10.1016/j.biomaterials.2014.10.018.

[15] X. Wu, B. Wang, Y. Li, X. Guan, M. Yin, W. Lv, Y. Chen, F. Lu, T. Qin, H. Gao, W. Jin, Y. Huang, C. Li, M. Gao, J. Lu, NIR driven catalytic enhanced acute lung injury therapy by using polydopamine@Co nanozyme *via* scavenging ROS, Chin. Chem. Lett. 36 (2025) 110211. https://doi.org/10.1016/j.cclet.2024.110211.

[16] H. Lee, S.M. Dellatore, W.M. Miller, P.B. Messersmith, Mussel-Inspired Surface Chemistry for Multifunctional Coatings, Science 318 (2007) 426–430. https://doi.org/10.1126/science.1147241.

[17] I.S. Kwon, C.J. Bettinger, Polydopamine nanostructures as biomaterials for medical applications, J. Mater. Chem. B. 6 (2018) 6895–6903. https://doi.org/10.1039/C8TB02310G.

[18] W. Lei, C. Sun, T. Jiang, Y. Gao, Y. Yang, Q. Zhao, S. Wang, Polydopamine-coated mesoporous silica nanoparticles for multi-responsive drug delivery and combined chemo-photothermal therapy, Mater. Sci. Eng. C. 105 (2019) 110103. https://doi.org/10.1016/j.msec.2019.110103.

[19] X. Li, C. Xie, H. Xia, Z. Wang, pH and Ultrasound Dual-Responsive Polydopamine-Coated Mesoporous Silica Nanoparticles for Controlled Drug Delivery, Langmuir 34 (2018) 9974–9981. https://doi.org/10.1021/acs.langmuir.8b01091.

[20] P. Sun, Z. Li, D. Zhang, W. Zeng, Y. Zheng, L. Mei, H. Chen, N. Gao, X. Zeng, Multifunctional biodegradable nanoplatform based on oxaliplatin prodrug cross-linked mesoporous polydopamine for enhancing cancer synergetic therapy, Chin. Chem. Lett. 35 (2024) 108346. https://doi.org/10.1016/j.cclet.2023.108346.

[21] W. Zeng, Z. Li, Q. Huang, C. Ding, L. Yang, W. Wang, Z. Shi, Y. Yang, H. Chen, L. Mei, X. Zeng, Multifunctional Mesoporous Polydopamine-Based Systematic Delivery of STING Agonist for Enhanced Synergistic Photothermal-Immunotherapy, Adv. Funct. Mater. 34 (2024) 2307241. https://doi.org/10.1002/adfm.202307241.

[22] A.D. Tripathi, Y. Labh, S. Katiyar, A.K. Singh, V.K. Chaturvedi, A. Mishra, Folate-Mediated Targeting and Controlled Release: PLGA-Encapsulated Mesoporous Silica Nanoparticles Delivering Capecitabine to Pancreatic Tumor, ACS Appl. Bio Mater. 7 (2024) 7838–7851. https://doi.org/10.1021/acsabm.4c00019.

[23] H. Song, C. Su, W. Cui, B. Zhu, L. Liu, Z. Chen, L. Zhao, Folic Acid-Chitosan Conjugated Nanoparticles for Improving Tumor-Targeted Drug Delivery, Biomed Res. Int. 2013 (2013) 723158. https://doi.org/10.1155/2013/723158.

[24] J. Zhang, B. Zhan, Y. Du, N. Liu, S. Liu, X. Li, Targeted cancer treatment using folic acid-functionalized carbohydrate polymers: A new era in nanomedicine, Ind. Crop. Prod. 235 (2025) 121704. https://doi.org/10.1016/j.indcrop.2025.121704.

[25] V.P. Torchilin, Multifunctional, stimuli-sensitive nanoparticulate systems for drug delivery, Nat. Rev. Drug Discov. 13 (2014) 813–827. https://doi.org/10.1038/nrd4333.

[26] E. Blanco, H. Shen, M. Ferrari, Principles of nanoparticle design for overcoming biological barriers to drug delivery, Nat. Biotechnol. 33 (2015) 941–951. https://doi.org/10.1038/nbt.3330.

[27] C. Wang, S. Ding, S. Wang, Z. Shi, N.K. Pandey, L. Chudal, L. Wang, Z. Zhang, Y. Wen, H. Yao, L. Lin, W. Chen, L. Xiong, Endogenous tumor microenvironment-responsive multifunctional nanoplatforms for precision cancer theranostics, Coord. Chem. Rev. 426 (2021) 213529. https://doi.org/10.1016/j.ccr.2020.213529.

[28] R. Jia, L. Teng, L. Gao, T. Su, L. Fu, Z. Qiu, Y. Bi, Advances in Multiple Stimuli-Responsive Drug-Delivery Systems for Cancer Therapy, Int. J. Nanomed. 16 (2021) 1525–1551. https://doi.org/10.2147/IJN.S293427.

[29] Z. Li, Z. Chen, K. Shi, P. Huang, W. Zeng, Q. Huang, J. Peng, L. Yang, H. Chen, Y. Zhao, X. Zeng, Polyphenol-Based Self-Assembled Nanomedicine for a Three-Pronged Approach to Reversing Tumor Immunosuppression, Adv. Healthcare Mater. 14 (2025) 2402127. https://doi.org/10.1002/adhm.202402127.

[30] A.-M. Șerban, I. Nacu, I. Rosca, A. Ghilan, A.G. Rusu, L.E. Niță, R.N. Darie-Niță, A.P. Chiriac, Preparation and Characterization of Polymeric Microparticles Based on Poly(ethylene brassylate-co-squaric Acid) Loaded with Norfloxacin, Pharmaceutics 16 (2024) 550. https://doi.org/10.3390/pharmaceutics16040550.

[31] A.P. Chiriac, A.G. Rusu, L.E. Nita, A.-M. Macsim, N. Tudorachi, I. Rosca, I. Stoica, D. Tampu, M. Aflori, F. Doroftei, Synthesis of Poly(Ethylene Brassylate-Co-squaric Acid) as Potential Essential Oil Carrier, Pharmaceutics 13 (2021) 477. https://doi.org/10.3390/pharmaceutics13040477.

[32] A.P. Chiriac, A. Ghilan, A.-M. Serban, A.-M. Macsim, A. Bargan, F. Doroftei, V.M. Chiriac, L.E. Nita, A.G. Rusu, A.-I. Sandu, Preparation of an Antioxidant Assembly Based on a Copolymacrolactone Structure and Erythritol following an Eco-Friendly Strategy, Antioxidants 11 (2022) 2471. https://doi.org/10.3390/antiox11122471.

[33] A.-M. Serban, A. Vieru, I. Rosca, I. Nacu, A.G. Rusu, A. Ghilan, L. Verestiuc, L.E. Nita, A.P. Chiriac, Development and Characterization of Levofloxacin-Loaded Vitamin A-Poly(Ethylene Brassylate-Co-Squaric Acid) Nanoemulsions, Macromol. Biosci. 25 (2025) e00088. https://doi.org/10.1002/mabi.202500088.

[34] B.D. da Silva, D.K.A. do Rosário, L.T. Neto, C.A. Lelis, C.A. Conte-Junior, Antioxidant, Antibacterial and Antibiofilm Activity of Nanoemulsion-Based Natural Compound Delivery Systems Compared with Non-Nanoemulsified Versions, Foods 12 (2023) 1901. https://doi.org/10.3390/foods12091901.

[35] W. Brand-Williams, M.E. Cuvelier, C. Berset, Use of a free radical method to evaluate antioxidant activity, LWT-Food Sci. Technol. 28 (1995) 25–30. https://doi.org/10.1016/S0023-6438(95)80008-5.

[36] D. Luong, P. Kesharwani, H.O. Alsaab, S. Sau, S. Padhye, F.H. Sarkar, A.K. Iyer, Folic acid conjugated polymeric micelles loaded with a curcumin difluorinated analog for targeting cervical and ovarian cancers, Colloids Surf. B Biointerfaces 157 (2017) 490–502. https://doi.org/10.1016/j.colsurfb.2017.06.025.

[37] İ. İnce, Y. Yıldırım, G. Güler, E.İ. Medine, G. Ballıca, B.C. Kuşdemir, E. Göker, Synthesis and characterization of folic acid-chitosan nanoparticles loaded with thymoquinone to target ovarian cancer cells, J. Radioanal. Nucl. Chem. 324 (2020) 71–85. https://doi.org/10.1007/s10967-020-07058-z.

[38] X. Yu, H. Fan, L. Wang, Z. Jin, Formation of Polydopamine Nanofibers with the Aid of Folic Acid, Angew. Chem. Int. Ed. 53 (2014) 12600–12604. https://doi.org/10.1002/anie.201404947.

[39] H. Fan, X. Yu, Y. Liu, Z. Shi, H. Liu, Z. Nie, D. Wu, Z. Jin, Folic acid–polydopamine nanofibers show enhanced ordered-stacking via π–π interactions, Soft Matter. 11 (2015) 4621–4629. https://doi.org/10.1039/C5SM00732A.

[40] A. Pezeshky, B. Ghanbarzadeh, H. Hamishehkar, M. Moghadam, A. Babazadeh, Vitamin A palmitate-bearing nanoliposomes: Preparation and characterization, Food Biosci. 13 (2016) 49–55. https://doi.org/10.1016/j.fbio.2015.12.002.

[41] K. Pramod, C.V. Suneesh, S. Shanavas, S.H. Ansari, J. Ali, Unveiling the compatibility of eugenol with formulation excipients by systematic drug-excipient compatibility studies, J. Anal. Sci. Technol. 6 (2015) 34. https://doi.org/10.1186/s40543-015-0073-2.

[42] T. An, N. Lee, H.-J. Cho, S. Kim, D.-S. Shin, S.-M. Lee, Ultra-selective detection of Fe^{2+} ion by redox mechanism based on fluorescent polymerized dopamine derivatives, RSC Adv. 7 (2017) 30582–30587. https://doi.org/10.1039/C7RA04107A.

[43] H. Luo, C. Gu, W. Zheng, F. Dai, X. Wang, Z. Zheng, Facile synthesis of novel size-controlled antibacterial hybrid spheres using silver nanoparticles loaded with poly-dopamine spheres, RSC Adv. 5 (2015) 13470–13477. https://doi.org/10.1039/C4RA16469E.

[44] H. Khosravi, R. Naderi, B. Ramezanzadeh, Synthesis and application of molybdate-doped mussel-inspired polydopamine (MI-PDA) biopolymer as an effective sustainable anti-corrosion substance for mild steel in NaCl solution, Biomass Convers. Biorefin. 14 (2024) 27557–27573. https://doi.org/10.1007/s13399-022-03514-w.

[45] M. Baibarac, I. Smaranda, A. Nila, C. Serbschi, Optical properties of folic acid in phosphate buffer solutions: the influence of pH and UV irradiation on the UV-VIS absorption spectra and photoluminescence, Sci. Rep. 9 (2019) 14278. https://doi.org/10.1038/s41598-019-50721-z.

[46] T. Tunç, C. Hepokur, A. Kariper, Synthesis and Characterization of Paclitaxel-Loaded Silver Nanoparticles: Evaluation of Cytotoxic Effects and Antimicrobial Activity, Bioinorg. Chem. Appl. 2024 (2024) 9916187. https://doi.org/10.1155/2024/9916187.

[47] A. Banstola, T.T. Pham, J.-H. Jeong, S. Yook, Polydopamine-tailored paclitaxel-loaded polymeric microspheres with adhered NIR-controllable gold nanoparticles for chemo-phototherapy of pancreatic cancer, Drug Deliv. 26 (2019) 629–640. https://doi.org/10.1080/10717544.2019.1628118.

[48] L. Chen, C. Chen, Y. Yan, L. Yang, R. Liu, J. Zhang, X. Zhang, C. Xie, Folic Acid Adjustive Polydopamine Organic Nanoparticles Based Fluorescent Probe for the Selective Detection of Mercury Ions, Polymers 15 (2023) 1892. https://doi.org/10.3390/polym15081892.

[49] D. Liu, X. Ding, J. Ding, J. Sun, Polypeptoid-Assisted Formation of Supramolecular Architectures from Folic Acid for Targeted Cancer Therapy with Enhanced Efficacy, Biomacromolecules 23 (2022) 2793–2802. https://doi.org/10.1021/acs.biomac.2c00166.

[50] A.P. Chiriac, E. Stoleru, I. Rosca, A. Serban, L.E. Nita, A.G. Rusu, A. Ghilan, A.-M. Macsim, L. Mititelu-Tartau, Development of a new polymer network system carrier of essential oils, Biomed. Pharmacother. 149 (2022) 112919. https://doi.org/10.1016/j.biopha.2022.112919.

[51] K. Ai, Y. Liu, C. Ruan, L. Lu, G.M. Lu, Sp2 C-Dominant N-Doped Carbon Sub-micrometer Spheres with a Tunable Size: A Versatile Platform for Highly Efficient Oxygen-Reduction Catalysts, Adv. Mater. 25 (2013) 998–1003. https://doi.org/10.1002/adma.201203923.

[52] D.R. Dreyer, D.J. Miller, B.D. Freeman, D.R. Paul, C.W. Bielawski, Elucidating the Structure of Poly(dopamine), Langmuir 28 (2012) 6428–6435.https://doi.org/10.1021/la204831b.

[53] H. Fan, X. Yu, Y. Liu, Z. Shi, H. Liu, Z. Nie, D. Wu, Z. Jin, Folic acid–polydopamine nanofibers show enhanced ordered-stacking via π–π interactions, Soft Matter. 11 (2015) 4621–4629. https://doi.org/10.1039/C5SM00732A.

[54] Y. Liu, G. Wu, L. Feng, J. Li, Y. Xia, W. Guo, K. Zhao, Harnessing Antioxidants in Cancer Therapy: Opportunities, Challenges, and Future Directions, Antioxidants 14 (2025) 674. https://doi.org/10.3390/antiox14060674.

[55] D.E. Uti, I.J. Atangwho, E.U. Alum, E. Ntaobeten, U.N. Obeten, I. Bawa, S.A. Agada, C.I.-O. Ukam, G.E. Egbung, Antioxidants in cancer therapy mitigating lipid peroxidation without compromising treatment through nanotechnology, Discov. Nano 20 (2025) 70. https://doi.org/10.1186/s11671-025-04248-0.

[56] M. Ghasemi, T. Turnbull, S. Sebastian, I. Kempson, The MTT Assay: Utility, Limitations, Pitfalls, and Interpretation in Bulk and Single-Cell Analysis, Int. J. Mol. Sci. 22 (2021) 12827. https://doi.org/10.3390/ijms222312827.

[57] A. Sukumaran, V.K. Sweety, B. Vikas, B. Joseph, A. Sukumaran, V.K. Sweety, B. Vikas, B. Joseph, Cytotoxicity and Cell Viability Assessment of Biomaterials, in: A. Sukumaran, M. A. Mansour (Eds.), Cytotoxicity - Understanding Cellular Damage and Response, IntechOpen, London 2023, pp. 1–24. https://doi.org/10.5772/intechopen.111822.

[58] M. Ahmadi, C.A. Ritter, T. von Woedtke, S. Bekeschus, K. Wende, Package delivered: folate receptor-mediated transporters in cancer therapy and diagnosis, Chem. Sci. 15 (2024) 1966–2006. https://doi.org/10.1039/d3sc05539f.